Tsunami risk modelling for Australia: understanding the impact of data

Graeme Hocking
Murdoch University

John Jakeman
Australian National University

Jane Sexton
Geoscience Australia

Matt Wand
University of Wollongong

1 Introduction

Modelling the impacts from tsunami events is a complex task. The approach taken by Geoscience Australia is a hybrid one where two models are combined. The first is one which models the earthquake rupture and subsequent propagation in deep water with the second propagating the tsunami through shallow water and focusing on subsequent inundation and impact ashore. The computer model ANUGA is used for the latter part of the approach and was developed collaboratively between the Australian National University and Geoscience Australia.

A critical requirement for reliable modelling is an accurate representation of the earth's surface that extends from the open ocean through the inter-tidal zone into the onshore areas. However, this elevation data may come from a number of sources and will have a range of reliability.

There are two questions that arise when data is requested. The first deals with the true variability of the topography, e.g. a flat surface needn't be sampled as finely as a highly convoluted surface. The second relates to sensitivity; how large is the error in the modelled output if the range of errors in the elevation data is known? ANUGA and similar models can take up days of computer time to simulate a particular scenario, and so full comparative tests for a range of input values is not viable. The main aim of this project was to understand the uncertainties in the outputs of the inundation model based on possible uncertainty in the input data.

2 The model

ANUGA is a model based on the shallow-water or depth integrated equations of fluid flow (see [10]). These are used in the form

$$h_t + (uh)_x + (vh)_y = 0 \tag{1}$$

$$(uh)_t + (u^2h + gh^2/2)_x + (vuh)_y + gh(z_x + S_{fx}) = 0 \quad (2)$$
$$(vh)_t + (vuh)_x + (v^2h + gh^2/2)_y + gh(z_y + S_{fy}) = 0 \quad (3)$$

where uh and vh are momentum in the x and y-directions, respectively, $z(x, y, t)$ is the bottom elevation, g is acceleration due to gravity, and $h(x, y, t)$ is the total water depth (above the terrain), so that $h(x, y, t)$ incorporates the contribution of the wave in addition to the existing depth of the water column. When the terrain represents the onshore elevation, $h(x, y, t)$ simply measures the height of water above the ground. The quantities S_{fx} and S_{fy} are the bottom friction modelled using Manning's resistance law as

$$S_{fx} = \frac{u\eta^2(u^2 + v^2)^{1/2}}{h^{4/3}} \text{ and } S_{fy} = \frac{v\eta^2(u^2 + v^2)^{1/2}}{h^{4/3}}$$

where η is the Manning resistance coefficient. The three model equations can be simplified to two by subtracting the mass conservation terms, but it is in the form given that they are solved in the model.

The model equations (1)-(3) are solved on a variable triangular mesh over the region of interest using a finite volume method. There are a number of models of similar type described in the literature using both this approach and the Boussinesq equations. These have been verified across a wide range of situations by comparison with both experimental and field data, to the extent that it is clear that the models do a good job of predicting the flow in shallow water, (or when the wavelength clearly exceeds the water depth), and subsequent runup of the tsunami wave [5, 8, 9, 11, 17]. This particular model (ANUGA) consequently has been shown to be accurate for a series of flow simulations including dam breaks and tsunamis [10].

These facts allowed the Mathematics and Statistics in Industry Study Group (MISG) group to assume the model to be sufficiently accurate to be used as a tool to determine the variations caused by errors in the input data. Variations in the runup of the tsunami can be treated as resulting purely from the changes in the input (topographic and wave) data, rather than from the model itself. This assumption also allowed us to consider using other similar models or even using analytic calculations to determine the variability due to variations in the input data.

3 Approach

The standard approach to finding the errors in a model of this kind is to perform a series of simulations varying the grid-spacing, time stepping and data inputs. Nonetheless, as stated above, this is not possible for the real situations under consideration because of time constraints. The best approach would therefore seem to be to follow the same process but with some much simpler scenarios that can be run quickly and easily. By necessity, these simulations were run on a coarse grid and with a greatly simplified geometry, and some more refined tests would need to be completed after the workshop to verify the conclusions. However, the results of these simple simulations may be assumed to be representative of the full simulations, and also to provide a framework for future tests outside of the time constraints provided by the MISG.

Therefore, the main activities undertaken by the workshop can be placed into four categories;

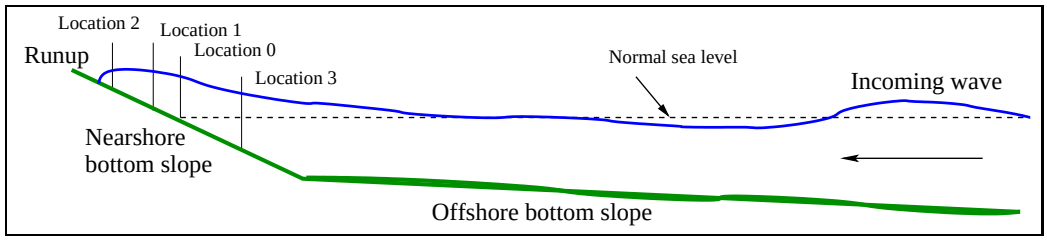

Figure 1: Simple one dimensional coastal scenario used in baseline simulations

- Sensitivity analysis using simple one and two dimensional situations to compute a table of first and second order variations in each output given each input, testing both sensitivity and nonlinearity.
- Monte Carlo simulations, using a simple model scenario, in which a random distribution of a particular input about some mean value was used in the simulation, and then considering the distribution of the output quantities.
- Consideration of other models to see if some simple or analytic expressions could be derived for the error.
- Determination of the sampling locations to adequately resolve the bottom topography.

In order to address the first three, the group decided on a scenario with a simple plane beach along a 50m wide strip, extending 2000m offshore, with two piecewise linear segments; one approaching the shore and one running up onto the inundation zone, see Figure 1. The bottom segment furthest out from the shore was also perturbed by a sinusoidal function to provide some variation away from a simple slope. To allow some two dimensional effects, some simulations involved a lateral, sinusoidal perturbation as well. Using this simple case, simulations ran in a matter of seconds. Due to the time constraints of the one week workshop, the activities outlined above were carried out in parallel, so it was not possible to use the results of one approach to refine the others.

In order to compare the results of the simulations, a measure is required, such as the inundation extent. As ANUGA uses an unstructured triangular mesh, the mesh vertices do not run parallel to the beach and so it was not possible to compare the extent of inundation directly between simulations unless an extremely fine grid was employed. This measure was used initially and an error of magnitude equal to the local grid resolution became evident in trial runs. Therefore, it was decided to measure the maximum ocean elevation at several points along the middle of the strip from just above the normal ocean level to just offshore within the inundation zone. The maximum elevation at these points can therefore be used as a proxy for runup. The four locations chosen are illustrated in Figure 1, and identified as Location 0, at the usual shoreline, Location 1, 0.55m above the shoreline, Location 2, 1.22m above the usual shore level, and Location 3 at 2.44m below the shoreline. The elevations at these locations are denoted as h_0, h_1, h_2 and h_3 respectively, and the horizontal velocities at these locations are denoted by v_0, v_1, v_2 and v_3.

3.1 Sensitivity assessment

Perhaps the most successful approach considered at MISG was a process in which the rate of variation of the outputs was computed from a series of simulations in which each of the input data values in turn was perturbed about some control value. This is sometimes called a first and second order local sensitivity assessment [12]. In other words, a very simple scenario was considered and the outputs computed. Then, in turn, each of the parameters of interest was varied by a small amount, in this case by $\Delta_5 = 0.5\%$ of the control value, while all others were kept at the control value. This gives an approximation to the local dependence of the model outputs on each of the individual inputs, or a first derivative of the model outputs with respect to each of the model inputs - a Jacobian matrix. Thus, if $H(I_C)$ is the value of the output parameter at the control value, where I is the input parameter, then

$$\frac{\delta H}{\delta I} \approx \frac{H(I_C + \Delta_5 I) - H(I_C)}{\Delta_5 I}$$

gives an approximation to the rate at which H changes as I is varied.

For example, if we choose the input parameter to be the bottom slope, the inundation level could be computed at a particular value of slope, the slope changed slightly and then the inundation recalculated. The change in inundation level is an estimate of how strongly the output depends on this particular input. This can then be repeated for other factors.

A second series of simulations with a variation of $\Delta_{25} = 0.25\%$ was also conducted. This allows an approximation to the second derivative to be calculated for the output dependence on each factor and hence provides an estimate of the degree of nonlinearity in the response. If this estimate is zero, then the response is linear. Using standard centered differences, this means that

$$\frac{\delta^2 H}{\delta I^2} \approx \frac{H(I_C + \Delta_5 I) - 2H(I_C + \Delta_{25}) + H(I_C))}{(\Delta_{25} I)^2}$$

provides an estimate for the nonlinearity of the relationship between H and I.

The parameters to be tested were bottom friction, input wave height, bottom slope, wavelength of the bottom oscillation and amplitude of the bottom oscillation. In the first two test cases, no variation was allowed in the lateral direction. The model consequently solved what is essentially a one dimensional problem. The "full" simulation took a matter of seconds and so output data were easily generated.

Two cases were considered using this one dimensional test. In the first, the control parameters were; bottom slope $S_B = 1/40$, input wave amplitude $A_I = 1$m, Manning friction coefficient $\eta = 0.01$, bottom oscillation amplitude $A_B = 1$m and bottom oscillation wavelength $\lambda_B = 100$m. The values selected are representative of tsunami; the bottom slope is reasonable for many nearshore beach slopes and tsunami amplitudes of 1m are entirely plausibly in 100m water depth. The Manning friction coefficient is representative of the nearshore bottom slope, (often η is given the value of 0.015 for smooth terrains such as grasslands, 0.03 for built up areas and 0.07 for landscapes with densely covered forest, therefore the value selected for η in this work is representative of the nearshore environment). Tsunami typically have much longer wavelength than that chosen here, however, for the purposes of the exercise and to speed up computations, a much shorter wavelength was used (otherwise a much larger computational domain would have been required). The input wave at the outer boundary (the right hand boundary in Figure 1) had the form $A_I \sin \omega t$ with $A_I = 1$m and $\omega = 1/100$. A range of input waves could have been selected here and the sine wave was chosen for its

simplicity and is often used to compare with the non-breaking analytical solutions of Carrier and Greenspan [3]. Other options include solitary waves and N-waves as suggested by Tadepalli and Synolakis [15]. It must be noted here that the purpose of the exercise was to develop a methodology for investigating sensitivity that will be applied to tsunami examples in the future and thus regardless of the type of the input wave, the methodology still stands. The bottom oscillation wavelength was chosen to be long compared to the local grid spacing so that it was accurately represented. The results are shown in Tables 1 and 2. Table 1 is the numerically approximated Jacobian, while Table 2 shows computations of the second derivative and hence shows the nonlinearity. In each case, the row that contains the largest absolute numbers is the dominant influence on the output variables.

Jacobian	h_0	h_1	h_2	h_3	v_0	v_1	v_2	v_3
Bottom Friction	-0.0000	-0.0000	-0.0000	-0.0000	-0.0001	0.0001	0.0002	-0.0002
Input Wave Amplitude	0.0240	0.0340	0.0478	0.0114	0.0485	0.0678	0.0900	0.0308
Bottom Oscillation Period	-0.0005	-0.0008	-0.0011	-0.0002	0.0011	0.0011	0.0003	0.0007
Bottom Slope	-0.0018	-0.0024	-0.0033	-0.0009	0.0030	0.0028	0.0025	0.0022
Bottom Oscillation Amplitude	0.0003	0.0004	0.0006	0.0001	0.0005	0.0011	0.0013	0.0002

Table 1: Jacobian matrix - Run 1. The dominant row is 'Input Wave Amplitude'.

	h_0	h_1	h_2	h_3	v_0	v_1	v_2	v_3
Bottom Friction	0.0007	0.0031	0.0072	0.0014	0.0527	-0.0975	-0.3048	0.2510
Input Wave Amplitude	-39.4539	-55.9124	-78.5101	-18.0534	-77.4300	-112.8141	-147.7459	-49.6513
Bottom Oscillation Period	0.8779	1.2916	1.8720	0.3607	-0.9700	-0.8461	0.4121	-0.7944
Bottom Slope	2.6535	3.6376	4.9962	1.4277	-6.9591	-6.6874	-5.5659	-4.8113
Bottom Oscillation Amplitude	-0.4357	-0.6279	-0.8973	-0.1959	-0.9226	-1.0726	-2.4443	-0.2227

Table 2: Second derivative (Nonlinearity) matrix - Run 1. The dominant row is 'Input Wave Amplitude'.

The second test series used the values; bottom slope $S_B = 1/20$, incoming wave amplitude $A_I = 1$m, Manning friction coefficient $\eta = 0.02$, bottom oscillation amplitude $A_B = 2$m, bottom oscillation wavelength $\lambda_B = 50$m. The incoming wave was chosen as above. The results are shown in Tables 3 and 4.

Jacobian	h_0	h_1	h_2	h_3	v_0	v_1	v_2	v_3
Bottom Friction	-0.0000	-0.0000	0.0025	-0.0000	-0.0003	-0.0044	-0.0039	-0.0002
Input Wave Amplitude	0.0486	0.1116	0.4889	0.0157	0.0973	0.0422	0.2110	0.0576
Bottom Oscillation Period	0.0007	0.0018	0.0080	0.0002	0.0034	-0.0005	0.0049	0.0018
Bottom Slope	-0.0009	-0.0020	-0.0080	-0.0003	0.0109	0.0017	-0.0042	0.0082
Bottom Oscillation Amplitude	0.0003	0.0008	0.0031	0.0001	0.0001	0.0001	0.0017	-0.0000

Table 3: Jacobian matrix - Run 2. The dominant row is 'Input Wave Amplitude'.

In both of these one dimensional scenarios, it is clear that the row that measures the changes due to variation in incoming wave amplitude, A_I, is an order of magnitude larger than the variation due to the other input variables that are related to the topography. If substantiated across the spectrum of parameter values, this is a very significant result, because it implies that unless the amplitude of the incoming wave is known very accurately, the error in the simulation of inundation will be dominated by the uncertainty in this factor.

In a third test case, a lateral (alongshore) oscillation in the bottom topography was included, as shown with significant vertical exaggeration in Figure 2. The width of the region

Non-Linearity	h_0	h_1	h_2	h_3	v_0	v_1	v_2	v_3
Bottom Friction	-0.0112	-0.03783	2.0222	-0.0027	-0.2286	-3.5136	-3.0792	-0.1509
Input Wave Amplitude	38.6997	88.8546	403.7461	12.5231	78.3693	33.8159	153.7179	46.2542
Bottom Oscillation Period	0.5592	1.4251	6.2283	0.1357	2.6693	-0.2462	3.8037	1.5023
Bottom Slope	-0.7503	-1.6836	-6.6934	-0.2673	9.2542	0.4028	-3.4113	6.4378
Bottom Oscillation Amplitude	0.2585	0.5990	2.4468	0.0797	0.0295	0.2014	1.3887	-0.0191

Table 4: Second derivative matrix - Run 2. The dominant row is 'Input Wave Amplitude'.

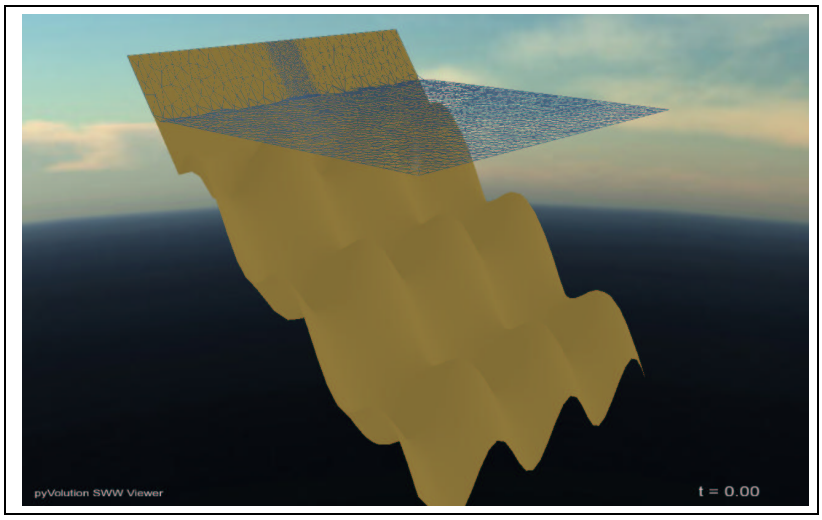

Figure 2: Diagram of the simulation geometry with lateral oscillations in the bottom bed.

was increased to $2000m$ so that some lateral effects could be seen. The onshore component was still broken into two components, and the inshore component was not perturbed laterally. This gives a first pass at determining the effect of lateral variations on the model outputs. The control was computed using the first case above with the added lateral perturbation with amplitude of $A_L = 1$m and a bottom wavelength of $\lambda_L = 100$m.

Again, as in the one dimensional cases, it was found that the amplitude of the incoming wave was the dominant factor by an order of magnitude on the value of the outputs. It also, again, turned out to be the term that exhibited the most nonlinear response.

This test needs to be performed over a range of control parameter values to ensure that there are no special cases. For example, there may be a bottom oscillation wavelength that will resonate with the wavelength of the incoming wave, causing significant steepening. In addition, one must be mindful that these tests do not take into account sudden bathymetric changes or focusing effects from the coastline; two dimensional effects that may cause "catastrophic" changes in the inundation. However, these tests can be repeated easily and quickly over the full range of possible inputs, and hence some reliability can be determined about the results.

3.2 Monte Carlo simulations

This series of tests was implemented as a comparison with the results above, and was performed in parallel. A similar coastal shape scenario was used to that above, but the simula-

Jacobian	h_0	h_1	h_2	h_3	v_0	v_1	v_2	v_3
Bottom Friction	0.0000	0.0000	0.0000	0.0000	-0.0003	-0.0007	-0.0008	-0.0004
Input Wave Amplitude	0.0247	0.0328	0.0545	0.0117	0.0428	0.0579	0.0970	0.0289
Bottom Oscillation Period	0.0003	0.0005	0.0008	0.0001	0.0020	0.0021	0.0010	0.0014
Bottom Slope	-0.0004	-0.0005	-0.0009	-0.0002	0.0034	0.0027	0.0030	0.0031
Bottom Oscillation Amplitude	0.0001	0.0001	0.0002	0.0000	0.0003	0.0002	0.0005	0.0001

Table 5: Jacobian with lateral oscillations. The dominant row is 'Input Wave Amplitude'.

Non-Linear	h_0	h_1	h_2	h_3	v_0	v_1	v_2	v_3
Input Wave Amplitude	-39.4822	-53.3244	-89.0271	-18.6628	-69.7723	-93.6795	-163.0223	-46.6794
Bottom Slope	0.6532	0.8762	1.4873	0.3573	-4.8038	-5.0484	-5.0257	-4.5641
Bottom Friction	-0.0216	-0.0297	-1.5316	-0.2278	-0.8917	0.0905	1.0824	-1.5286
Bottom Oscillation Period	-0.5747	-0.8426	-1.5316	-0.2278	-0.8917	0.0905	1.0824	-1.5286
Bottom Oscillation Amplitude	-0.1246	-0.1660	-0.2769	-0.0568	-0.1736	-0.4351	-0.9721	-0.2110

Table 6: Second derivative with lateral oscillations. The dominant row is 'Input Wave Amplitude'.

tions were performed with a number of randomized variations in the input parameters. This method is known as probabilistic Monte-Carlo simulation [12] and is shown schematically in Figure 3. The drawback of this approach is the large number of simulations that must be performed to determine a representative distribution. The advantage is that a much wider variation in each parameter can be considered in a series of simulations, for example a 20% variation around a particular value rather than the 0.5% considered in the above tests.

In this approach, the value of one input parameter was varied in a random, but normally distributed fashion while all other input values were held fixed. The idea is that this would be repeated for each of the input values. During the MISG a series of simulations were conducted in which the wavelength of the bottom bathymetry perturbation was varied about a mean of $\lambda_B = 100$ with a standard deviation of $s(\lambda_B) = 20$, using the `Python` normal/random distribution. Again, the maximum height of water above each of the test locations was recorded as for the one dimensional test case.

The randomly simulated distribution of input values seen in Figure 4 suggests that more simulations than time permitted at MISG are required to achieve a normal distribution. However, we were still able to draw some preliminary conclusions.

The distribution of the resultant maximum water depths at each of the four test locations is shown in Figure 5. The main outcome of the four plots shown is that the variance in the water depth is extremely small in comparison with the variance in the input (period of the

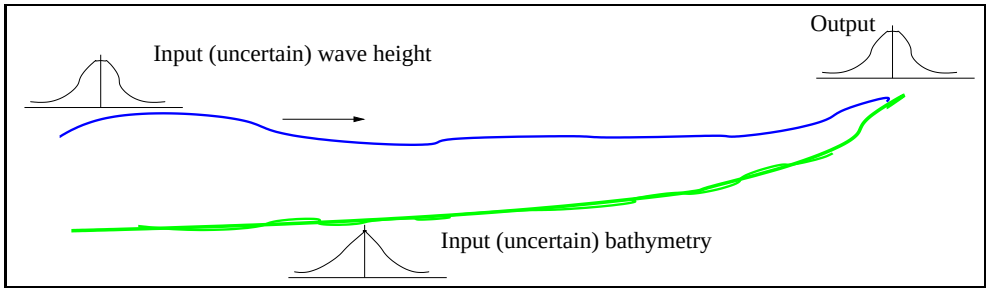

Figure 3: Schematic of sensitivity test method 2

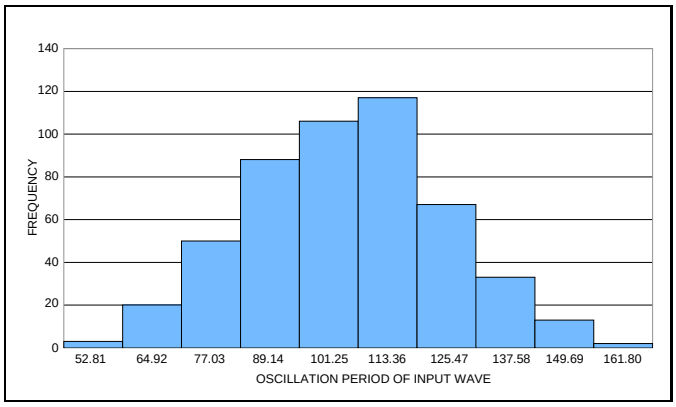

Figure 4: Distribution of input wave periods for the Monte-Carlo simulation

seafloor disturbance). This outcome aligns with the results from the previous section in that the period of the bottom oscillation had minimal effect on the outputs.

Time did not permit a comparison of the normalised variance of the input and output and it is recommended that this be considered in future work. Additionally, further investigation is required to determine the nature of the peaks and whether the bi-modality persists for more simulations. The random selection of the wavelength from a normal distribution will select values close to the mean and the small standard deviation selected here may be a result of the high peaks seen in Figure 5. Future work could investigate stratified sampling that also allows the consideration of extreme values. Further work should also incorporate an investigation of the grid resolution to determine whether this has affected the asymmetry in the plots shown in Figure 5 and additionally separate the results into more than ten bins.

This approach is computationally slower in comparison to the one described in section 3.1. Further tests investigating the response to an input distribution of initial wave amplitude, bottom slope, oscillation etc. should be a good comparison with the first sensitivity analysis and should be able to confirm or disprove the inferences of that test.

3.3 Other models

There is a large body of work on the shallow water equations that could be studied to better understand the situation under consideration. For example, [3] used a transformation to compute the exact solution to the one-dimensional case for flow up a linear slope, while [4] and [16] considered runup over variable topography. [14] found a semi-analytic solution using a series method, again for a linear bottom slope, while [8] computed solutions with a series of combined linear segments for the bottom slope. Other numerical models have been used to assess errors and compare with experimental and field data. For example, [5] showed that errors in the cross-shore boundary conditions dissipated in the wave-breaking zone near to the beach and recommended that an accurate model needed to be applied over a length scale of around 10 times the width of this zone.

All of this earlier work shows clearly that the numerical models using the shallow water equations (or in some cases the Boussinesq approximation) provide good estimates not only of runup but also wave shape, e.g. [17] (field) or [14] (experimental).

The analytical solutions could be used to assess the effect of errors in some of the factors

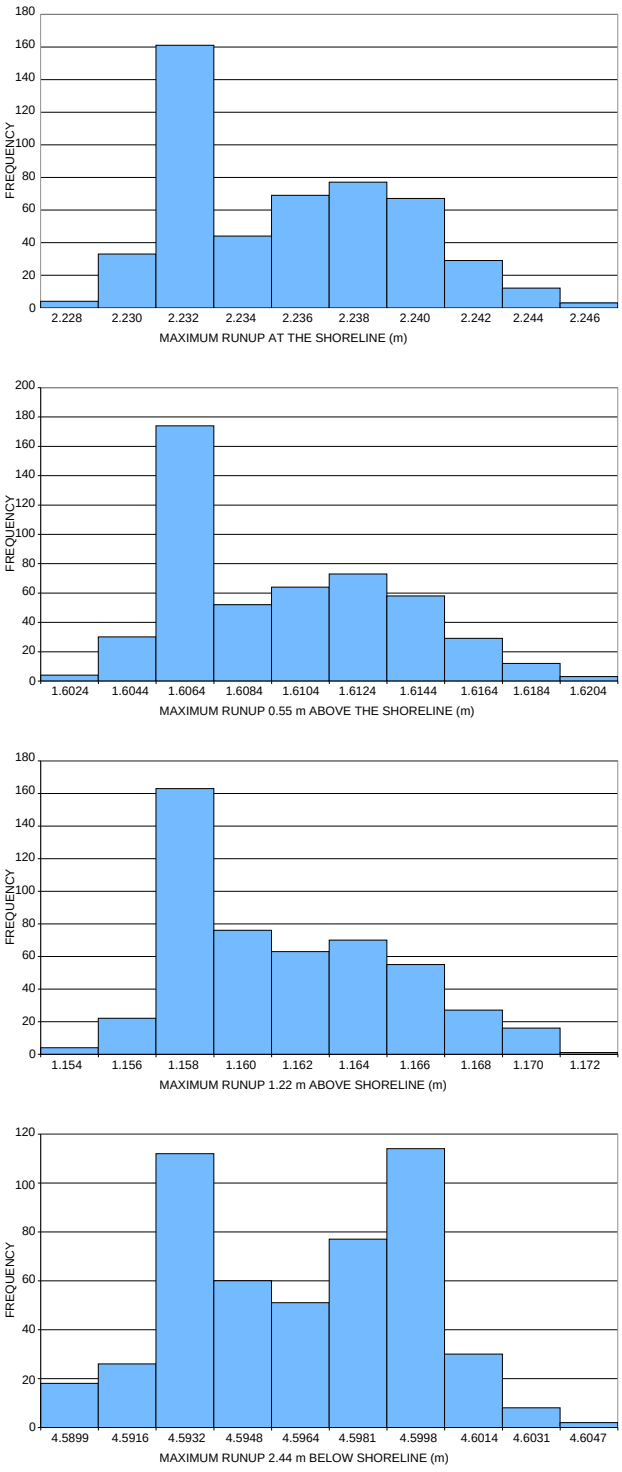

Figure 5: Frequency distribution of maximum water level at the 4 locations; (a) at the usual shoreline, (b) 0.55m above (c) 1.22m above (d) 2.44m below the usual shoreline.

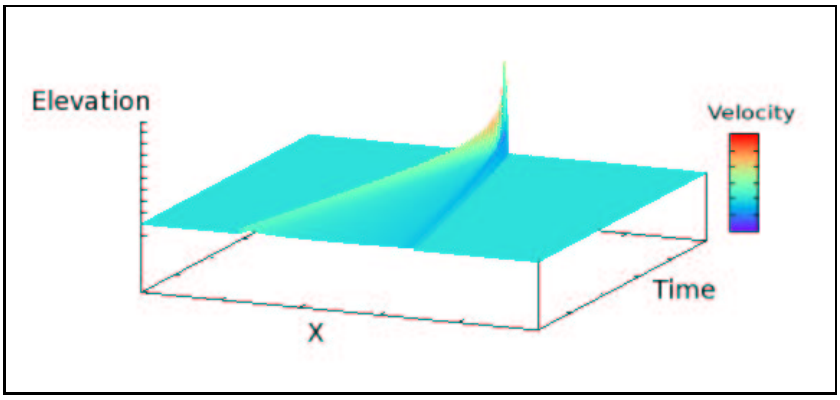

Figure 6: The time evolution of a tsunami wave with no initial velocity using [7]. Time is moving toward the reader. Colours indicate magnitude of water velocity. The vertical scale is greatly exaggerated.

in which we are interested, while there also exist simple versions of one dimensional solvers for the shallow water equations that could be used in a similar manner to obtain fast and accurate sensitivity results, e.g. `clawpack` [2] or the more specific `tsunamiclaw`, [6]. Alternatively, a much more detailed model, such as that of [7], which solves the two dimensional Navier-Stokes equations (through a vertical slice running onshore) with a Smagorinsky model of turbulence, could be used. During the MISG, some simulations were performed with both `clawpack` and the model of [7] to compare with the sensitivity analyses using ANUGA, with encouraging results. A typical simulation using this latter model is given in Figure 6.

The model `clawpack` was used to perform some preliminary tests to consider the variation in inundation as several of the major input parameters were altered. The case considered was a single, linear slope (with only one segment this time) in which the bottom slope was $S_B = 1/50$, the amplitude of the incoming wave was half of the bottom depth at the outer limit, and no bottom friction was included (so it is a worst case scenario). Tsunami amplitudes in the open water do not have this characteristic but can occur once the tsunami shoals in the nearshore environment. As before, this value was selected for testing purposes only. The effect of incoming wave amplitude, incoming wavelength and bottom slope can be seen in Figure 7. Given that this model is based on the same equations as ANUGA, the relationship would be the same. Clearly as the incoming wave amplitude or wavelength increases, the inundation level increases, and at a similar rate. This is to be expected because in both cases there is an increase in the mass of water in the wave. However, it does mean that the wavelength needs to be incorporated into the sensitivity simulations. The effect of increasing bottom slope is to cause a decrease in inundation, but this is also to be expected since more energy is required to push the water up the slope. These simulations do show how this model or even a semi-analytic model could be used to investigate the parameter space without having to set up simulations using the full ANUGA model.

3.4 Omissions

The MISG work group was unable to consider several aspects of the problem that were originally considered of interest. In particular, we did not consider the sampling required to

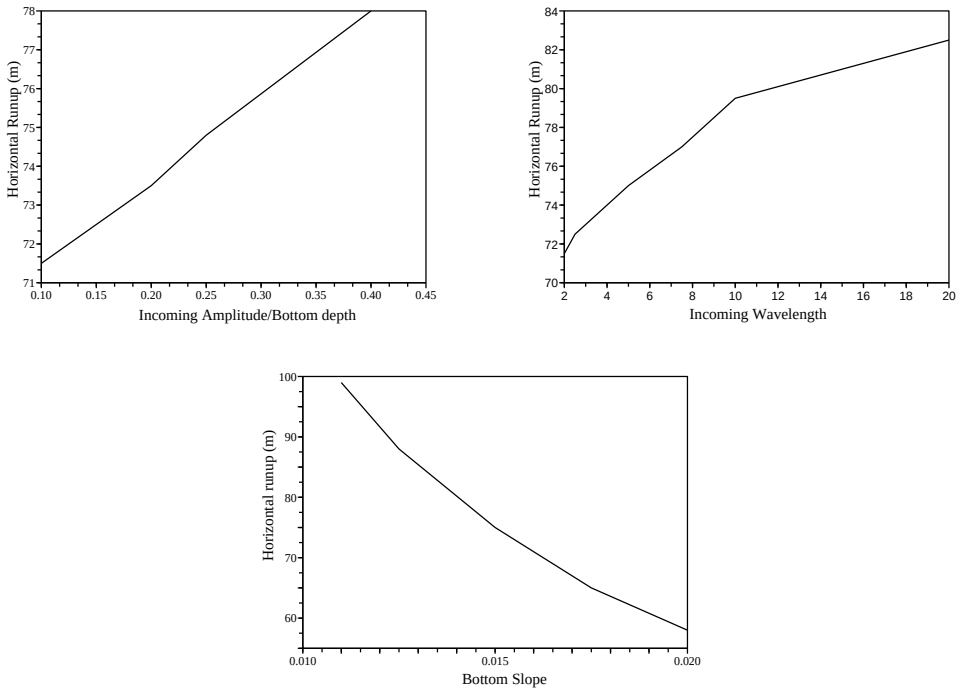

Figure 7: Simulations performed using `clawpack`, showing change in runup while varying (a) incoming amplitude, (b) wavelength and (c) bottom slope

correctly resolve the bottom topography sufficiently given the desired accuracy of the model. This requires further research and statistical input. The sampling required to adequately resolve the bottom of an uncharted bay does indeed depend on the variation in depth of the bay itself. There is no point in measuring on a scale smaller than the resolution of the model. In fact, if the test results above are replicated over a wide range of scenarios, it may not be necessary to have particularly accurate topographical resolution, as the main source of error is in the incoming wave. It seems likely that except for large vertical obstacles, unless the variation is of an order significant compared to the wavelength of the incoming wave, it is likely to have little impact. However, the location and movement of sandbars may cause significant variations in the topography, and their effect is under consideration for future work.

4 Outcomes and further work

The main outcome of the MISG workshop was the methodology to investigate the sensitivity of the tsunami inundation model to a range of inputs. That is, the variation in the model output can be determined by calculating the first and second derivatives with respect to variations in inputs. This methodology can be implemented as part of Geoscience Australia's tsunami risk modelling program.

The results of the MISG week have pointed to several options for further investigation. Continuation of both the one dimensional and two dimensional sensitivity analyses at different

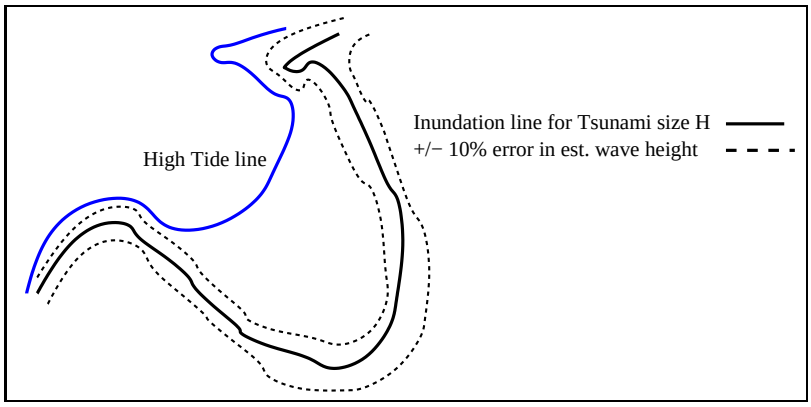

Figure 8: Schematic of what an inundation map with errors might look like.

locations in the parameter space is required to verify the initial findings. Inclusion of the sensitivity to the wavelength of the incoming wave also seems necessary and wavelengths appropriate to the shallow water wave equations must be selected (the wavelength used in this initial exercise is not valid in this context). This could be done by proceeding in a similar manner to that outlined above, or could be followed up using similar techniques in the analytic solutions, i.e. compute the Jacobian matrix analytically from the equations. Automatic differentiation techniques as described by [13] could also be investigated.

In addition, further work is required to understand how sudden bathymetric changes or focusing or reflections from islands or other coastal features affect runup calculations. The presence of seasonal movement of sandbars should also be considered as well as any focusing of the wave by the coastline. All of these tests, however, can be done using the simple one and two dimensional scenarios described above rather than full simulations. These idealised cases should be verified against full models when available. [1] have used ANUGA to study how tsunami run-up is affected by a range of coastal embayment types. Whilst they did not investigate sensitivity specifically, the results indicate that the bathymetry does play an important role in predicting tsunami impact. Continuation of studies similar to this will determine the parameters that lead to the greatest sensitivity. These studies will need to follow a probabilistic analysis approach whereby a range of scenarios are investigated.

Another conclusion of the MISG group is that *for simple cases*, the effect of relative errors in estimates of the amplitude of the tsunami are large in comparison to the effects of the other input errors, e.g. topographic errors. If the error in the input wave is understood then three simulations could be conducted to understand the sensitivity to the input wave only. The three simulations would be one with the given input wave and the remaining two with the input wave $\pm$ the error as shown in Figure 8. In addition to understanding the sensitivity to the input wave, the simulations would highlight how the topography under consideration responds, i.e. is the topography inherently vulnerable to wave attack? This will lead to an increased understanding for what problems bathymetry and topography are important.

Conducting tsunami risk assessments in Australia will continue to rely on the validation of the tsunami risk modelling methdology. This process is ultimately linked to having a complete understanding of the likelihood and mechanisms of the tsunamigenic earthquake. This requires a program to understand the history of tsunami through palaeotsunami research both in Australia and within the region, as well as more improved rupture models. The

question remains on the required accuracy and spatial resolution of the supporting elevation data.

Acknowledgements

The moderators would like to thank the industry representative, Jane Sexton, from Geoscience Australia, and the others who contributed to the discussions and work on this problem; Simon Clarke, Dian Georgiev, Songping Zhu, Melanie Roberts, Steve Roberts, Lewis Mitchell, Kate Snow, Fatimah Noor Harun and John Cogill.

References

[1] Baldcok, T.E., Barnes, M.P., Guard, P.A., Hie, T., Hanslow, D., Ranasinghe, R., Gray, D. & Nielsen, O. (2007) Modelling tsunami inundation on coastlines with characteristic form, *Proc. 16th Austral. Fluid Mech. Conf.*

[2] Berger, M.J. & LeVeque, R.J. (1998) Adaptive Mesh Refinement Using Wave Propagation Algorithms for Hyperbolic Systems, *SIAM J. Numer. Anal.* **35**, 2298-2316.

[3] Carrier, G.F. & Greenspan, H.P. (1958) Water waves of finite amplitude on a sloping beach, *J. Fluid Mech.*, **4**, 97-109.

[4] Carrier, G.F. (1966) Gravity waves on water of finite depth, *J. Fluid Mech.*, **24**, 641-659.

[5] Chen, Q. & Svendsen, A. (2003) Effects of cross-shore boundary conditions errors in nearshore circulation modelling, *Coastal Engng.*, **48**, 243-256.

[6] George, D.L. (2006) *Finite Volume Methods and Adaptive Refinement for Tsunami Propagation and Inundation*, PhD Thesis, University of Washington, see `http://www.math.utah.edu/~george/tsunamiclaw.html`

[7] Georgiev, D., Roberts, A.J. & Strunin, D. (2007) The dynamics of the vertical structure of turbulence in flood flows, *ANZIAM J.*, **48**, C573-C590.

[8] Kânoğlu, U. & Synolakis, C.E. (1998) Long wave runup on piecewise linear topographies, *J. Fluid Mech.*, **374**, 1-28.

[9] Lynett, P.J., Wu, T-R. & Liu, P.L-F. (2002) Modeling wave runup with depth-integrated equations, *Coastal Engng.*, **46**, 89-107.

[10] Nielsen, O., Roberts, S., Gray, D., McPherson, A. & Hitchman, A. (2005), Hydrodynamic modelling of coastal inundation, *MODSIM 2005, Int. Cong. Modelling and Simulation*, 518-523.

[11] Pelinovsky, E., Troshina, E., Golinko, V. & Petrukhin, N. (1999) Runup of tsunami waves on a vertical wall in a basin of complex topography, *Phys. Chem Earth (B)*, **24**, 431-436.

[12] Saltelli, A., Chan K. & Scott E.M., Eds, (2000), *Sensitivity analysis*, John Wiley and Sons Ltd., West Sussex, England.

[13] Sambridge, M., Rickwood, P., Rawlinson, N. & Sommacal, S. (2007) Automatic differentiation in geophysical inverse problems, *Geophys. J. Int.*, **170**, 1-8.

[14] Synolakis, C.E. (1987) The runup of solitary waves, *J. Fluid Mech.*, **185**, 523-545.

[15] Tadepalli, S. & Synolakis, C.E. (1994), The run-up of N-waves on sloping beaches, *Proceedings: Mathematical and Physical Sciences*, **445**, 1923, 99-112.

[16] Tuck, E.O. & Hwang, L. (1972) Long wave generation on a sloping beach, *J. Fluid Mech.*, **51**, 449-461.

[17] Zahibo, N., Pelinovsky, E., Talipova, T., Kozelkov, A. & Kurkin, A. (2006), Analytical and numerical study of nonlinear effects at tsunami modelling, *Appl. Maths & Computation*, **174**, 795-809.